Journal of Structural Geology Vol 13, No 9, pp 1001 to 1011, 1991
Printed in Great Britain

0191-8141/91 $03 00+0 00

An experimental steady-state foliation

J H. Ree

Department of Geological Sciences, State University of New York at Albany, 1400 Washington Ave , Albany, NY 12222, U S A

(Received 29 August 1990, accepted in revised form 30 April 1991)

Abstract—The history of the intensity and orientation of a grain shape foliation was investigated in octachloropropane deformed in simple shear at 80% of its absolute melting temperature and a shear strain rate of 4×10^{-5} s^{-1} Foliation orientation, developed from the beginning of the deformation, remains steady throughout the deformation Foliation intensity becomes steady after a bulk shear strain of about 0 9 has been accumulated The steadiness of foliation orientation and intensity is achieved by some balance between foliation strengthening and foliation weakening processes The main foliation strengthening process is intragranular plastic deformation. Foliation weakening processes include dynamic recrystallization by migration of straight or slightly wavy grain boundaries, grain dissection, rotational recrystallization, grain amalgamation, relative rigidity of hard grains and grain boundary sliding A small but definite angle, although not constant, is observed between the foliation and the long axis of the bulk total strain ellipse The average aspect ratio of grains is lower than that of the bulk total strain ellipse by a factor of about 0 4 at total shear strain of 1 3 The average grain size also stabilizes, becoming steady from a shear strain of 0 5 onwards A steady grain shape foliation may be a possible paleostress or a paleostrain rate indicator, but cannot be a paleostrain indicator

INTRODUCTION

Grain shapes in deformed rocks have been used extensively as strain indicators (e.g Ramsay & Huber 1983, fig. 7.16, Odling 1984), and grain-shape foliations have been used as sense of shear indicators (e.g. Ramsay & Graham 1970, Berthé *et al.* 1979, Simpson & Schmid 1983, Lister & Snoke 1984). However, there has been little study of the complete history of grain shapes or the foliation defined by them in naturally or experimentally deformed materials. Some partial histories of foliation development have been recorded in rock analog materials (Means 1981) and in ice (Burg *et al.* 1986). But steady-state foliation, which remains steady in both orientation and intensity throughout an interval of deformation (Means 1981), has not yet been directly observed in any material The study of structures insensitive to the finite strain, like steady-state foliation, is important because such structures are potential indicators of the orientation and intensity of the steady-state flow stress or of the strain rate. I illustrate an example here of a steady-state foliation and the history of its development in octachloropropane, C_3Cl_8 (hereafter called OCP) deformed in simple shear at 80°C or 80% of its absolute melting temperature (160°C) and at 4×10^{-5} s^{-1} shear strain rate, using synkinematic microscopy (Means 1989). OCP is a soft, hexagonal organic material Optically it has similar looking microstructures to quartz and has been used in several previous microstructural studies (see Ree 1990 and references therein). The techniques of synkinematic microscopy and information about the apparatus are given by Means (1989).

Foliation in rocks can be defined by compositional layering, grain size variation, discontinuities, preferred orientation of grain boundaries, and preferred orientation of platy minerals or lenticular mineral aggregates (Hobbs *et al.* 1976, p 213) In this experimental example, the foliation is a grain shape foliation, defined statistically by the preferred orientation of long axes of grains (*foliation orientation*) and the ratio of long axes to short axes of grains (*foliation intensity*)

EXPERIMENTAL TECHNIQUES

The sample was a mixture of OCP and 1000 grit silicon carbide particles, prepared as explained by Jessell (1986) and Means & Ree (1988). Passively moving silicon carbide particles within the OCP serve as material marker points that allow strain calculation and recognition of grain boundary migration. Photomicrographs in plane and cross-polarized light with an objective lens of ×4 magnification were taken every 30 min during the deformation. During each recording, four photographs in cross polarized light were taken at four different positions of the nicols relative to the specimen in order to show all grain and subgrain boundaries. Photomicrographs with an objective lens of ×20 magnification were also taken every hour in the central part of the sample, for a more precise record of the microstructure and marker particle positions

The orientations of *c*-axes of the grains were measured on a universal stage before and after deformation. During the deformation they were measured by using the flat stage extinction direction (for the trend of the *c* axis) and birefringence measurement with a Berek compensator (for the plunge of the *c*-axis) Although the accuracy of *c*-axis plunge measurement with a Berek compensator (with an error range of ±10°, Ree unpublished data) is not as good as on a universal stage, we can follow the approximate reorientation trajectories of

c axes without interrupting the deformation (Ree 1990). Bulk strain of the sample was determined by averaging strains indicated by displacement of 10 sets of three widely spaced marker particles, with a distance of about 0.9–1.6 mm between marker particles in a set. The imposed bulk deformation was not ideal simple shearing but an approximate simple shearing with a small shortening across the shear zone. A bulk shear strain in this paper represents the value of D_{12} of the average deformation tensor D_{ij} (Means 1990) with the X axis parallel to the direction of the bulk shearing or the direction of the relative displacement of the upper part of the shearing sample and the Y axis normal to it.

For a quantitative analysis of grain shape foliation, grain boundaries of the individual grains were digitized from enlarged photographs at the scale of about 123:1, using an Hitachi digitizing tablet coupled to an IBM-PC. The bulk shear direction, again, was taken as the X axis with the Y axis normal to it. All directions were measured counterclockwise from the dextral shear direction. To digitize grain boundaries, co-ordinates of points were read at 2 mm intervals along the grain boundaries in the photographs. This corresponds to a true length interval of 16 μm. To obtain the statistical orientation and intensity of foliation, these data were processed with a QUICKBASIC program, GBO, employing the projection method modified from Panozzo (1983). All segments of grain boundaries were projected onto the projection axis (x axis) initially parallel to the shear direction (X axis). The projection was reiterated for each position of the projection axis rotated counterclockwise from the shear direction by an increment of 1° through an angle of 180°. As explained later, the ratio of the longest projection ($A(\alpha)_{max}$, α = rotation angle of the x axis) to the shortest projection ($A(\alpha)_{min}$), and the orientation of $A(\alpha)_{max}$ coincide with the ratio of the longest to shortest axes of grains and the preferred orientation of the grain longest axes, respectively. The method and procedure are described by Panozzo (1983, 1984) and Schmid *et al.* (1987) in more detail.

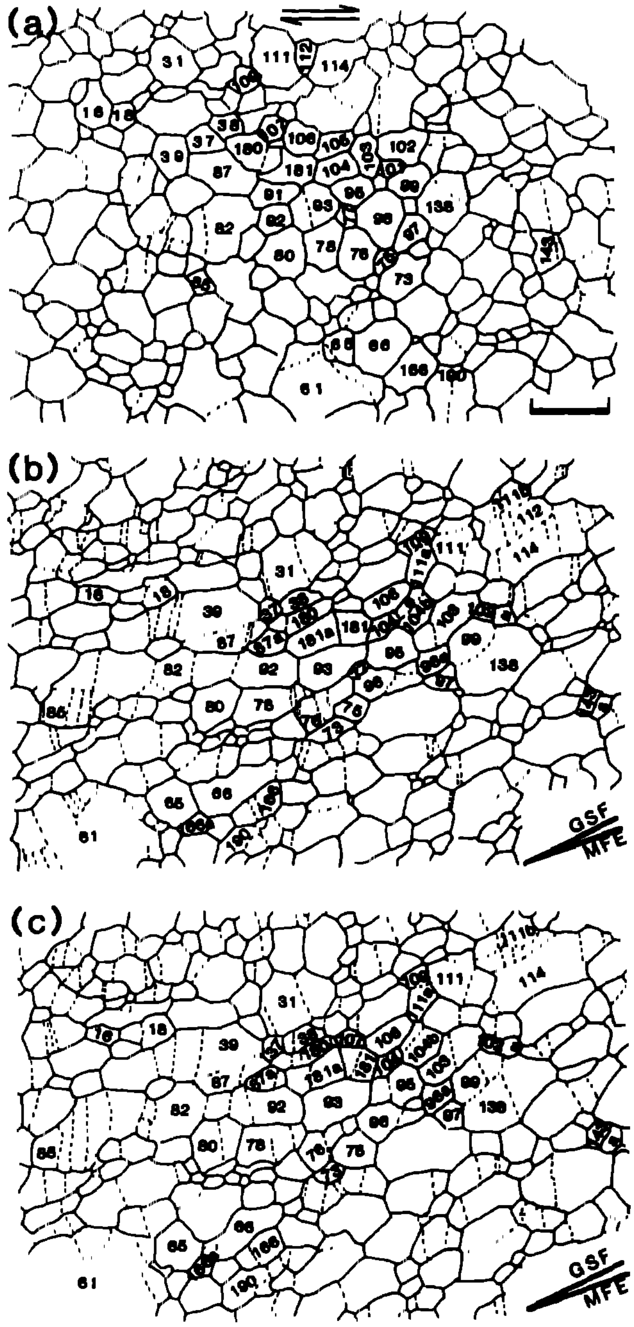

Fig. 1. Maps of OCP sample TO 110, showing solid lines as grain boundaries and dashed lines as subgrain boundaries. Grains referred to in the text and shown in the detailed map of Fig. 9 are numbered. Arrows at the top show the sense and direction of shear. (a) Microstructure immediately before deformation. (b) Microstructures 9.5 h later, immediately after deformation with a bulk shear strain of 1.3. (c) Microstructures after a static interval of 22 h after deformation. Scale bar in the right bottom of (a) corresponds to 250 μm. Orientations of grain shape foliation (GSF) and maximum finite elongation (MFE) are indicated in (b) and (c). Standard deviations of these orientations are about 30° and 2°, respectively.

OBSERVATIONS AND ANALYSES

The sample at the beginning of the deformation (Figs. 1a and 2a) shows a foam texture consisting of optically strain-free, equiaxed grains. The average grain area is about 9.8×10^{-3} mm^2. Loading the sample at 80 ± 5°C initiates deformation of the grains and grain boundary migration (Fig. 2b). The migrating grain boundaries are not generally serrated or lobate. Instead they are straight or slightly wavy in most cases. In some cases, they have large wavelength bulges with half wavelengths (bulge width) of the same order as the grain radius, as commonly seen in OCP deformed at lower temperature (Means 1983). Foliation does not become easily visible until a bulk finite shear strain of about γ = 0.4 has accumulated (Fig. 2c). From this strain onwards, the direction and intensity of foliation appear to be more or less steady to a total bulk shear strain of 1.3 (Figs. 2d–g). There is also some development of subgrain boundaries, most of which are approximately perpendicular to the shear zone boundary and parallel to the c axes of the grains (Fig. 1b). Although there is local increase in grain area by grain boundary migration and amalgamation, the average grain area of 12.3×10^{-3} mm^2 at the end of the deformation does not differ much from the initial average area. With 22 h of static interval

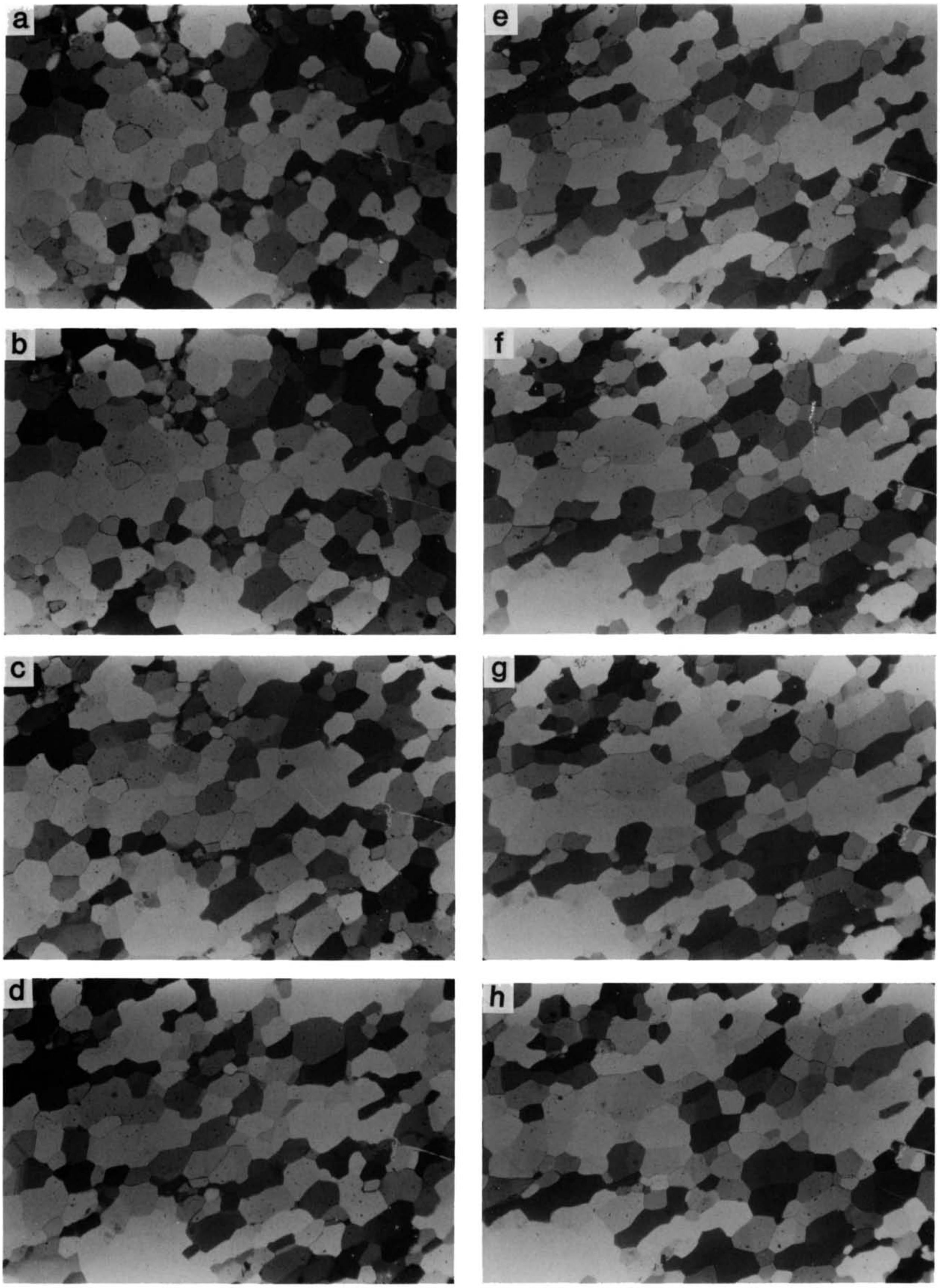

Fig. 2. Photomicrographs of the area mapped in Fig. 1 in cross polarized light. (a) before deformation. (b) during deformation with $\gamma = 0.1$, (c) $\gamma = 0.4$, (d) $\gamma = 0.6$, (e) $\gamma = 0.9$, (f) $\gamma = 1.2$. (g) after deformation, with $\gamma = 1.3$, and (h) after a static interval of 22 h after deformation. Fine black dots are marker particles. The dextral shear direction is horizontal. The length of each photograph corresponds to 1.96 mm.

after the deformation (this is twice the duration of the deformation), with the temperature unchanged, the foliation intensity and orientation still look 'frozen' without significant change (Figs 1c and 2h)

Deformation pattern

An imaginary square grid (Fig. 3a) is superimposed on the undeformed sample, and Jessell's (1986) triangle method was used to calculate, from displacements of the marker particles, the shape of this grid at the end of the deformation (Fig 3b) This apparently shows the imposed dextral simple shear deformation with local heterogeneities In the map of marker particle trajectories (Fig. 3c), it can be seen that marker particles are progressively displaced more or less parallel to the bulk shear direction except in two areas, one to the NW and the other to the SE of a fixed marker particle in the center (solid circle) In these two areas the marker particle trajectories show a somewhat hyperbolic pattern due to the existence of small shortening displacements across the shear zone

Reorientation of c-axes

The c axis fabric diagram at the beginning of the deformation is shown in Fig 4(a). Owing to the pressing of the sample between two glass slides perpendicular to the plane of observation, to obtain a desired sample thickness, and some preferential extrusion along the shear zone during sample pressing, preferred orientation of c axes has already been introduced before deformation With the deformation, the c axis fabric does not seem to change much from the beginning, although there is a strengthening of a single girdle of c axes, already developed normal to the shear direction, which is symmetric with respect to the bulk shear plane but asymmetric with respect to the grain-shape foliation (Fig. 4b). Figure 5 shows c axis reorientation trajectories of a few grains in the central area of the sample The c axes of grains in the NW and SE quadrants of the trajectory diagram rotate sympathetically to the imposed bulk simple shear, generally enhancing the single girdle fabric Those in the NE and SW quadrants show some complex rotations although they do not weaken the single girdle fabric.

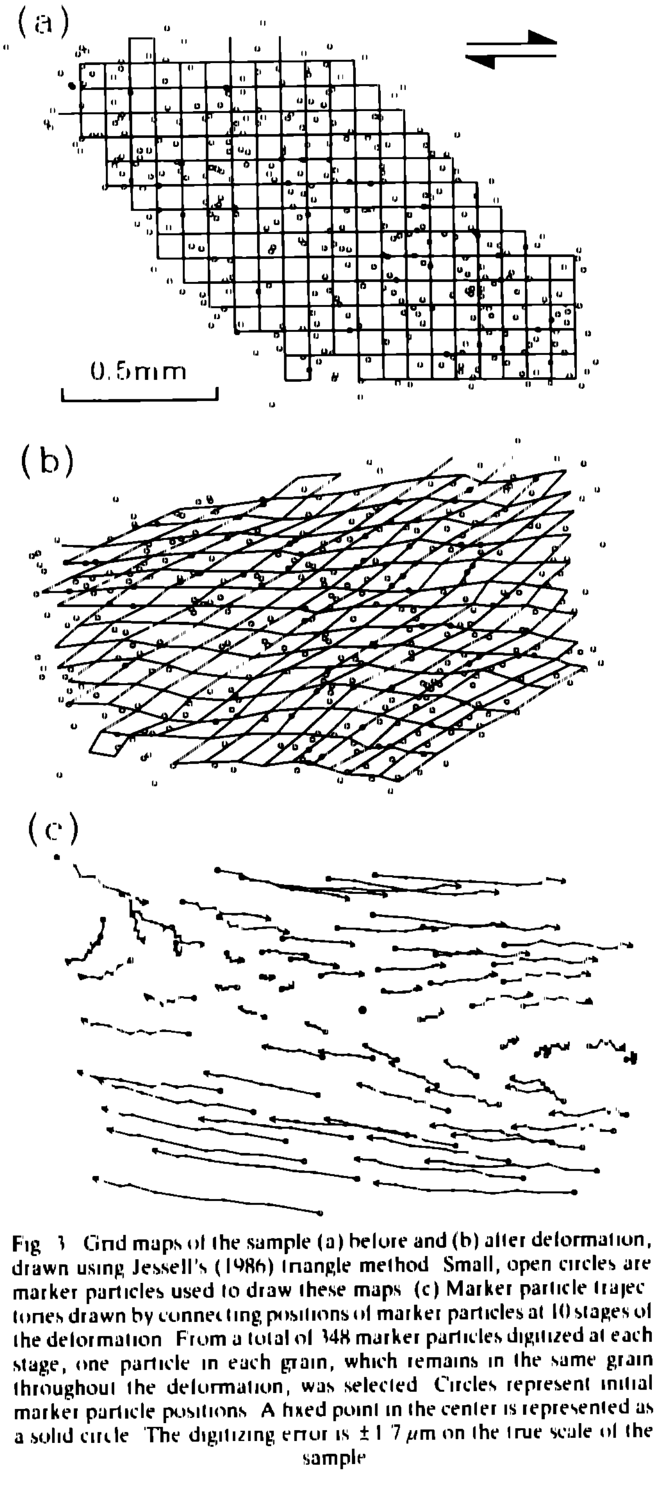

Fig 3 Grid maps of the sample (a) before and (b) after deformation, drawn using Jessell's (1986) triangle method Small, open circles are marker particles used to draw these maps (c) Marker particle trajectories drawn by connecting positions of marker particles at 10 stages of the deformation From a total of 348 marker particles digitized at each stage, one particle in each grain, which remains in the same grain throughout the deformation, was selected Circles represent initial marker particle positions A fixed point in the center is represented as a solid circle The digitizing error is ±1 7 μm on the true scale of the sample

Grain size history

For grain size measurement, the area of each grain was measured on the enlarged photographs by calculating the area enclosed by the digitized grain boundary. About 180 grains were measured at each stage, and average grain area was determined by dividing the total sum of grain areas measured by the number of grains The results are plotted against the bulk shear strain in Fig 6 The initial average area of 9.8×10^{-3} mm^2 increases by about 23% after a bulk shear strain of about 0.5 has accumulated. The average grain area of about 12.1×10^{-3} mm^2 becomes steady from this shear strain to the end of deformation Considering the relatively large standard deviation of grain area in Fig 6, however, the sample does not maintain an equigranular texture through the deformation Also, the preferred growth of some grains and shrinkage of other grains in Figs 1 and 2 indicate that the area of individual grains is not steady even though the average grain area of the sample is steady. During static recovery, there is slight increase in grain area of about 8%.

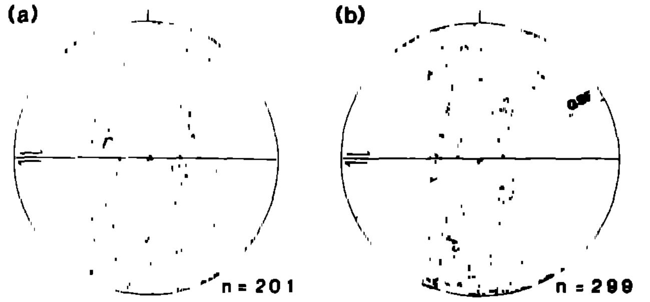

Fig. 4. c axis fabric diagrams of the sample (a) before and (b) after deformation. GSF in (b) represents grain shape foliation. The c axes of some grains outside the area mapped in Fig. 1 are also plotted. Lower hemisphere equal area projections.

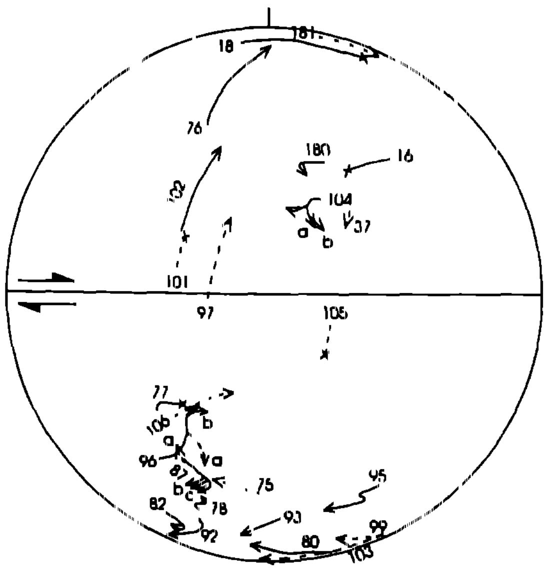

Fig. 5. c axis reorientation trajectories of the grains in the central part of the sample. Solid lines represent trajectories for which c axes were measured not only before and after deformation but also during deformation. Those for which c axes were measured only before and after deformation are indicated by dashed lines. Grains which disappeared during deformation have crosses at the end of their trajectories. See also Fig. 9 for intragranular strains of most grains in this diagram.

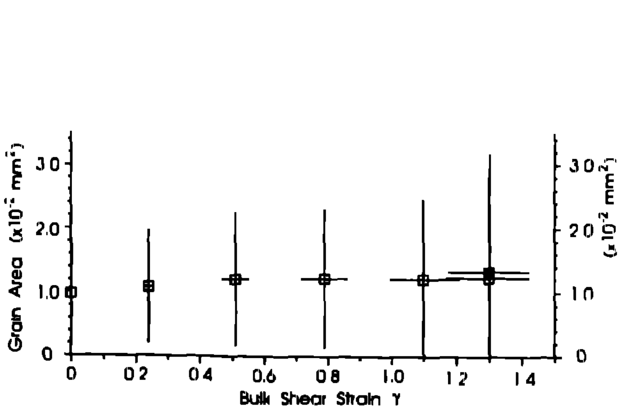

Fig. 6. Plots of average grain area vs bulk shear strain of the sample. The solid square represents the average grain area after a static interval of 22 h after deformation. Vertical and horizontal bars are ± 1 standard deviations for grain area and bulk shear strain, respectively.

Foliation history

Grain boundary orientation data are shown as rose diagrams representing the total length of grain boundaries per angle of orientation, and as projection diagrams representing the total length of projection ($A(\alpha)$) of grain boundaries per angle of rotation of x axis (α) in Fig. 7. The maximum and minimum value of $A(\alpha)$, $A(\alpha)_{max}$ and $A(\alpha)_{min}$, respectively, occur 87–95° apart at each stage, indicating that the projection functions are symmetric. Panozzo (1983, 1984) and Schmid *et al.* (1987) showed that the ratio of the longest projection ($A(\alpha)_{max}$) to shortest projection ($A(\alpha)_{min}$) and the orientation of $A(\alpha)_{max}$ coincide with the ratio of the longest to shortest axes of grains and the preferred orientation of the grain longest axes, respectively, if the following criteria are satisfied: (a) the rose diagram of grain boundary orientations is unimodal and symmetric; (b) the projection function is symmetric. Since the rose diagrams are more or less unimodal and symmetric, and the projection functions are symmetric in the sample (Fig. 7), we can use the projection method to get the average aspect ratio of the grains and the preferred orientation of the grain long axes.

Figure 8(a) shows plots of foliation intensity, defined here as the statistical ratio of long axis to short axis of grains, against the bulk shear strain (γ), and of the axial ratio of the bulk finite strain ellipse (R_f) against γ. Also shown is a plot of foliation intensity calculated as if the original grain boundary array had been passively deformed by a homogeneous deformation given by the bulk deformation at each stage. Initially the sample has equiaxed grains with almost no grain shape foliation (an intensity less than 1.1, Figs. 1a, 2a, 7a and 8a). With accumulating strain, foliation intensity increases slowly. The foliation becomes recognizable at $\gamma = 0.4$ (Fig. 2c) and its intensity is about 1.3 at this stage (Fig. 8a). The foliation intensity reaches its highest value (1.5) at $\gamma = 0.9$, and then becomes steady, although it decreases a little bit (less than 0.1) at the end of the deformation. Even after 22 h of static interval after the deformation, a period about twice as long as the duration of the deformation, there is almost no change in foliation intensity of 1.4. The axial ratio of the finite strain ellipse, R_f, on the other hand, increases rapidly from the beginning, being higher than foliation intensity by a factor of about 2.3 at $\gamma = 1.3$. The foliation intensity plot of the hypothetical, homogeneously deformed sample runs almost exactly parallel to the R_f plot, with only slightly higher values (≈ 0.1) than R_f. This difference results from the initial foliation intensity of about 1.1 at 24° in the undeformed sample.

The plot of foliation orientation against γ in Fig. 8(b) shows that the foliation orientation is steady at 25 ± 3° throughout the deformation. As with the foliation intensity, the foliation orientation does not change during the static interval after the deformation. The direction of maximum finite stretch (θ') decreases continuously with deformation, from 33° at $\gamma = 0.1$ to 20° at the end of the deformation. However, the difference between θ' and foliation orientation is less than 6° throughout the deformation. The foliation orientation curve of the homogeneously deformed sample runs almost parallel to the θ' curve, remaining only 2° less than θ' after reaching 27° at $\gamma = 0.35$.

PROCESSES FOR STEADY-STATE FOLIATION

Figure 9 shows maps of grain boundaries and intragranular strain in the central part of the sample. Intragranular strain was measured using the displacements of sets of three widely spaced marker particles within a grain and it is not necessarily homogeneous within a grain. In Fig. 9(a), a bulk shear strain of 0.1 has already been imposed. At the end of the deformation, which accumulated an additional bulk shear strain of 1.2, most of the grains show an aspect ratio lower than the R_i ratio of their intragranular strain ellipse (Fig. 9b), and also lower than the theoretical aspect ratio of the same grains deformed assuming passive grain boundaries (Fig. 9c). Some foliation weakening processes are evidently at work to limit the degree to which intragranular plastic deformation can produce a microstructure like that shown in Fig. 9(c). Several foliation weakening processes are seen to be operating in this sample and are discussed below. These are: migration recrystallization including migration of straight or slightly wavy grain boundaries and dissection, rotational recrystallization, amalgamation, rigidity of hard grains and grain boundary deformation mechanisms.

Migration of straight or slightly wavy grain boundaries weakens the foliation most effectively, by the slow migration of grain boundaries at a low angle to the grain long axis away from the grain center or grain boundaries at a high angle to the grain long axis toward the grain center. Examples are shown in Fig. 10 for grain boundaries between grains 92 and 93, between grains 78 and 80, and the NW boundaries of grains 80, 92 and 93. If there occurs migration of grain boundaries at a low angle to the grain long axis toward the grain center or grain boundaries at a high angle to the grain long axis away from the grain center, as in the NE boundary of grain 93 in Fig. 10, this process can strengthen the foliation, but this is not common in the sample. This kind of recrystallization is classed as continual grain boundary migration by Drury & Urai (1990) and as local grain boundary migration by Knipe & Law (1987), although the latter authors expect non steady-state foliation with this migration mechanism.

Dissection (Urai *et al.* 1986, Means 1989) weakens the foliation by dividing an elongated grain into separate, more equiaxed parts by growth across it of other grains (Fig. 11). Six grains are found to be dissected by other grains in the whole area mapped in Fig. 1. Although it was not found in the sample described here, another possible weakening process by grain boundary migration is the *coalescence* of two grains with similar lattice orientations which were not initially in contact with each other, leading to the development of a Type IV subgrain boundary of Means & Ree (1988). Foliation weakening occurs if coalescence of grains occurs along their short dimension. If coalescence of grains occurs along their long dimension, on the other hand, this process can strengthen the foliation.

Rotational recrystallization develops more equiaxed, smaller grains from an elongated grain by transforming low angle boundaries into high angle boundaries, if low angle boundaries are at a high angle to the grain long axis. A total of 16 grains in the whole area mapped in Fig. 1 behaved in this way and examples are grains 96 and 181 shown in Fig. 9. If high angle boundaries develop at a low angle to the grain long axis however, rotational recrystallization can strengthen the foliation (Fig. 12). But this strengthening process is generally rare in simple-shearing experiments on OCP and found for only one grain in the area mapped.

Amalgamation (Means 1989) is another possible weakening process, which turns grain boundaries at a low angle to the grain long axes into subgrain boundaries with progressive reduction of misorientation (grains 111b, 112 and 114 in Figs. 1a & b). These are called Type III subgrain boundaries by Means & Ree (1988). A total of nine grains were seen to amalgamate in this way in the sample. If amalgamation occurs along a grain boundary at a high angle to the grain long axis, however, it could strengthen the foliation. This occurred locally (grains 82 and 92 in Figs. 1a & b). Ribbon grains generally develop parallel to bulk shear direction in this way, here and in other simple shearing experiments on OCP, usually to develop a high strain zone.

Hard grains are unsuitably oriented for single slip on weak systems. They usually grow into globular grains without much intragranular strain but with rigid-body rotation (Ree 1990). Grains 61 in Fig. 1 and 95 in Fig. 9 are typical hard grains. Of a total of 148 grains in Fig. 1(a) whose *c* axes were measured, 17 grains are probable hard grains with their *c* axes parallel to or within 20° of the shortening direction, assuming the main shortening direction to be at about 45° to the shear direction. Of these 17 grains, intragranular strain measurement was possible for four grains which enclosed three or more specific marker particles throughout the deformation. These are grains 31, 61, 95 and 138 (see Fig. 1). All of these grains suffered much lower strain (R_i = 1.3–1.5) than the bulk strain (R_i = 3.3) and increased their grain area by about 60–140%. These grains weaken the foliation, although grain 138 would have looked more elongate if it had not amalgamated with grain 99 (Figs. 1a & b).

Grain boundary deformation mechanisms, especially grain boundary sliding, are also a weakening process if they are accompanied by more or less rigid translation of grains. Study of the displacement field of marker particles showed fault like features across grain boundaries at eight sites in Fig. 1, commonly around hard grains (Means & Ree 1990). The amount of offset is usually 70–80 μm, or 0.6–0.7 the average grain diameter. There may have been other, unrecognized grain boundary sliding sites where needed to partly accommodate strain hetero

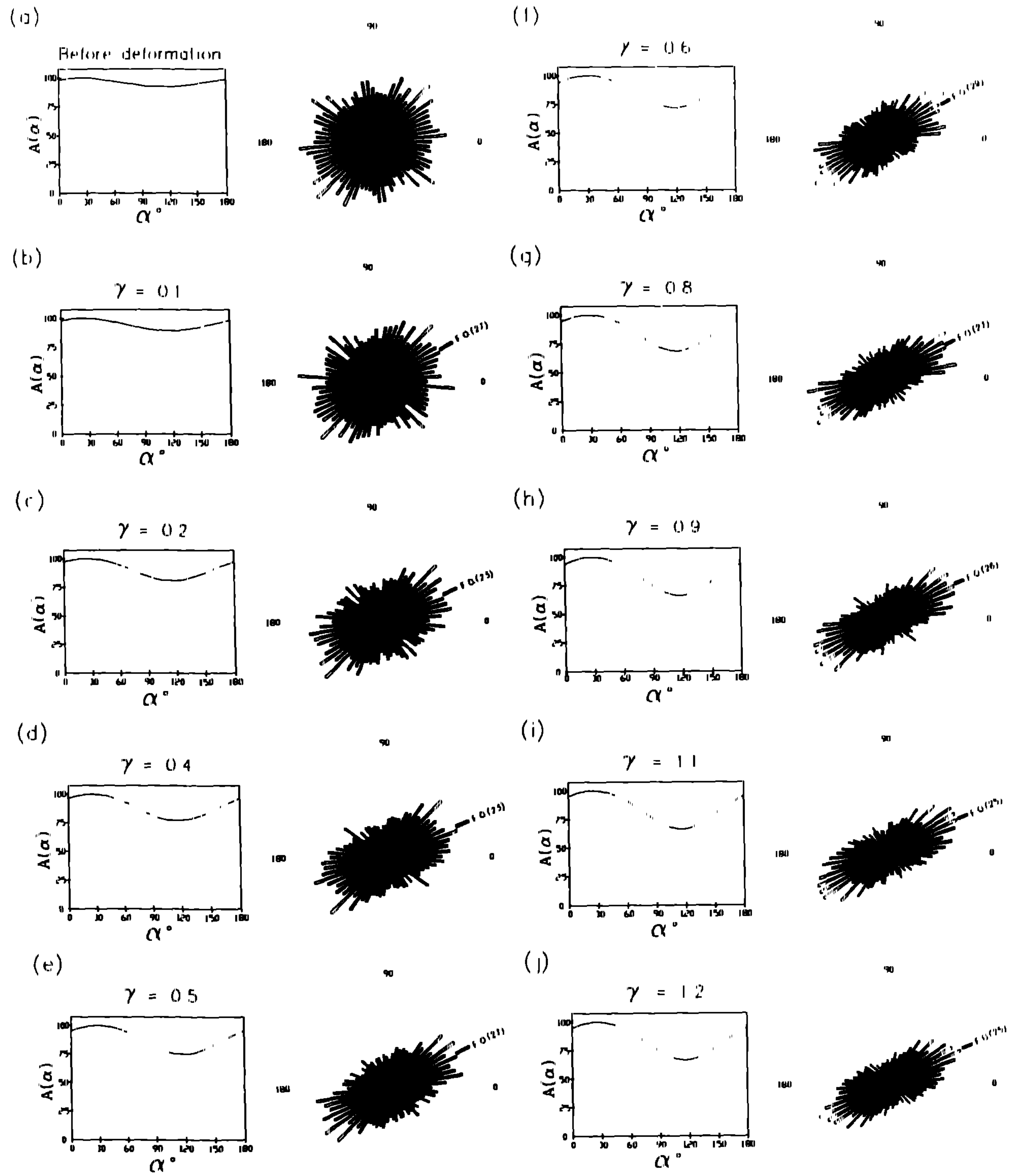

Fig. 7. Projection diagrams (left) and rose diagrams (right) of grain boundaries of the sample. The projection diagram represents the total length of grain boundaries projected onto the x axis per angle of rotation of the axis. The rose diagram represents the total length of grain boundaries per angle of orientation. F.O. in the rose diagram means foliation orientation.

geneities. But this weakening process is believed to have played only a minor role, considering the fact that the average intragranular strain calculated in Fig. 9(b) (R_f = 3.3) is nearly the same as the bulk strain.

Analysis of grain shape foliation was also carried out on two other experiments which showed more extensive grain boundary sliding and development of grain boundary openings (experiment TO 105, Ree 1988), and more extensive grain boundary migration (experiment TO 109, Ree 1990). In these experiments, the foliation orientations appear unsteady but the intensities are steady at a value of 1.1–1.2. With these low intensity values, however, the apparent unsteadiness of the orientation is of uncertain significance.

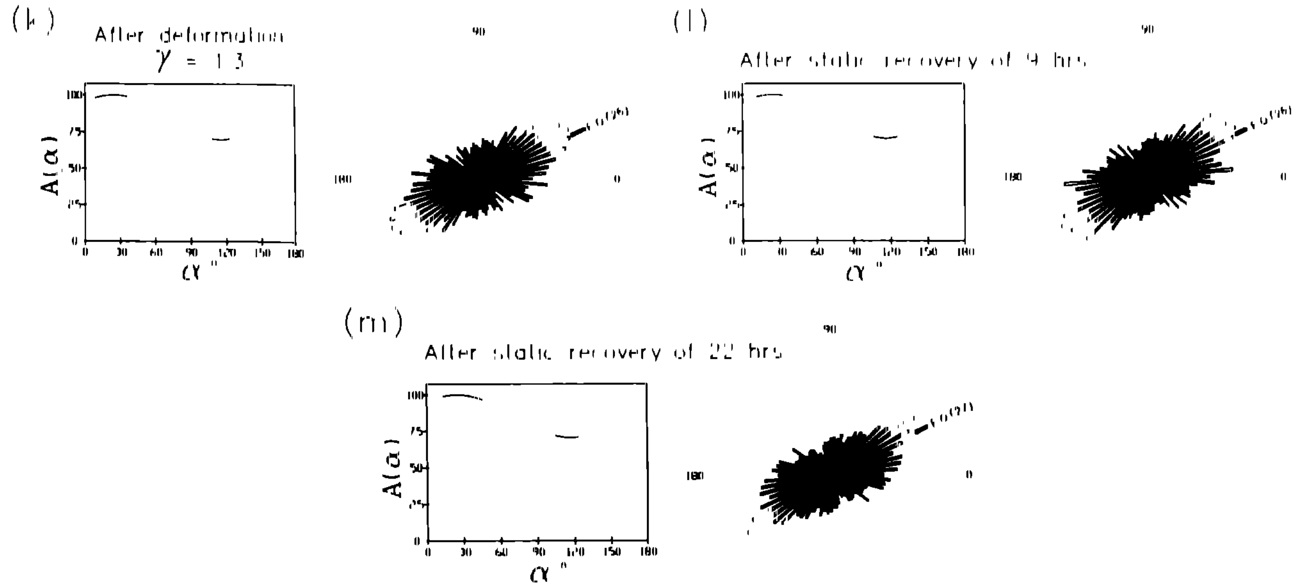

Fig. 7 (k-m)

CONCLUSION

With intragranular plastic deformation as a dominant foliation strengthening process, steady state foliation that has statistically constant orientation and intensity is achieved by several foliation weakening processes in the sample. The major foliation weakening process is dynamic recrystallization by grain boundary migration, which involves migration of straight or slightly wavy grain boundaries and grain dissection. Other processes include rotational recrystallization and grain amalgamation. Hard grains also weaken the foliation with their rigid behavior. Grain boundary sliding does not have any significant role as a foliation-weakening process although it does operate in several sites.

Retardation of the foliation intensity curve behind the strain ellipse curve is large, indicating that the determination of strain by grain shape is not useful where grain boundary migration is widespread, as has already been suggested by Means (1983) and Knipe & Law (1987). If grain shapes in the sample in Fig. 1(b), for example, are used for strain determination, the apparent R_f value will be lower than the true R_f value by a factor of about 0.4.

Lister & Snoke (1984), Law (1986) and Knipe & Law (1987) discussed the possible cyclic nature of steady state foliation, although they considered only the orientation of foliation. No major cycles are found in intensity and orientation of foliation in the experiment described here. Considering the large strains possible in naturally deformed rocks, however, the foliation behavior described in this paper may represent only a short-lived, beginning part of longer histories. Experiments, such as those using a ring shear apparatus, are needed for further study of foliation behavior at very large strains.

The main contribution of this study has been to demonstrate that steady state foliation is possible in deforming polycrystals, and to record the microstructural characteristics of one specific example.

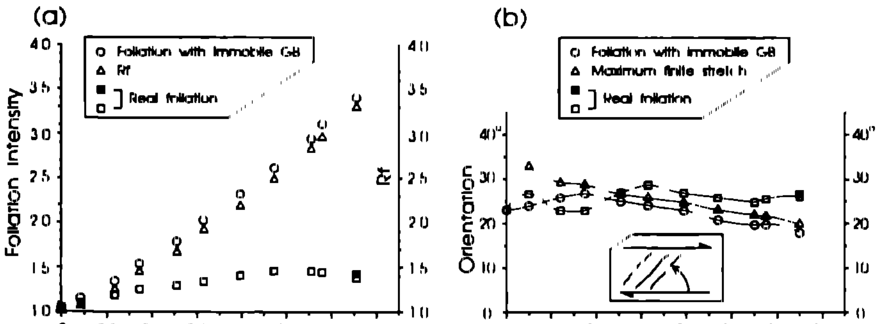

Fig. 8. (a) Plots of bulk shear strain vs foliation intensity (squares), R_f (triangles) and foliation intensity with homogeneously deformed, passive grain boundaries (circles). The solid square represents the foliation intensity after a static interval of 22 h deformation. The standard deviation of the bulk shear strain is the same as in Fig. 6. Standard deviations of foliation intensity at γ = 1.1 are about 0.4 for true foliation and less than 0.1 for imaginary foliation. Standard deviations of R_f are 0.1–0.4 for all the stages. (b) Plots of bulk shear strain vs orientations of true foliation (squares), imaginary foliation (circles) and maximum finite stretch (triangles). The standard deviations of foliation orientations at γ = 1.1 are about 30° for the true foliation and 5° for the imaginary foliation. Standard deviations of maximum finite stretch orientations are 2–4° for all stages.

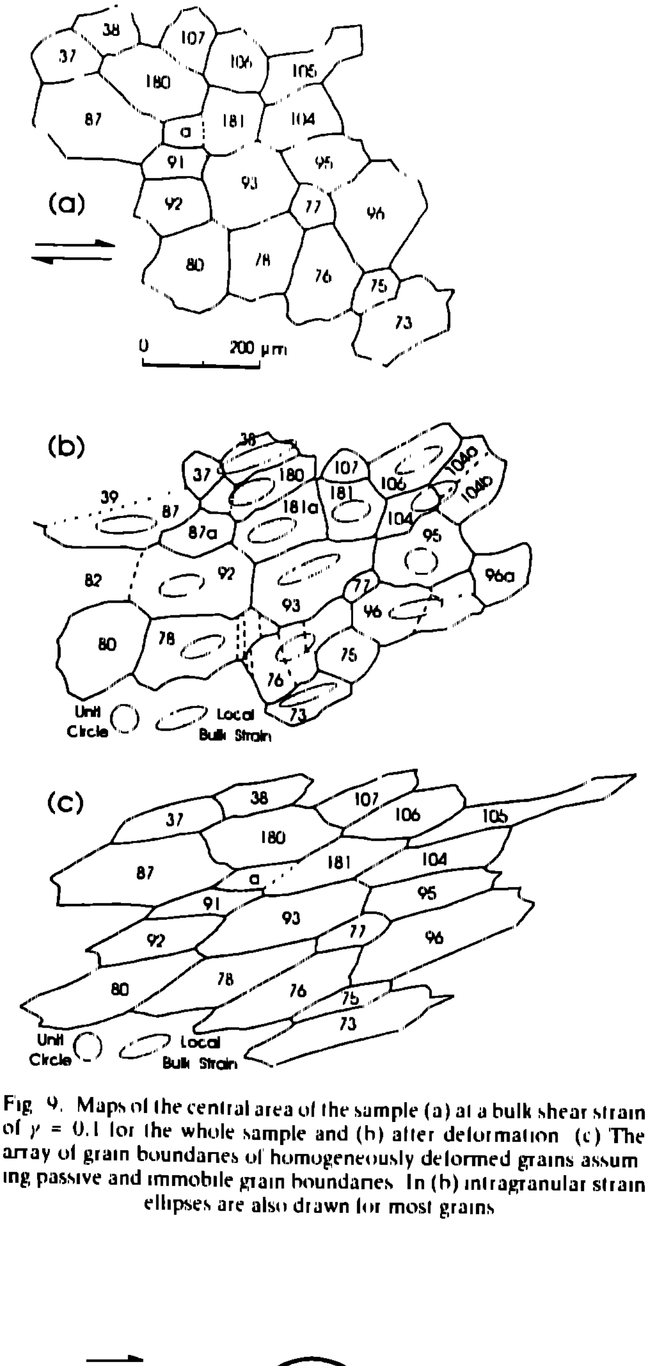

Fig 9. Maps of the central area of the sample (a) at a bulk shear strain of γ = 0.1 for the whole sample and (b) after deformation (c) The array of grain boundaries of homogeneously deformed grains assuming passive and immobile grain boundaries In (b) intragranular strain ellipses are also drawn for most grains

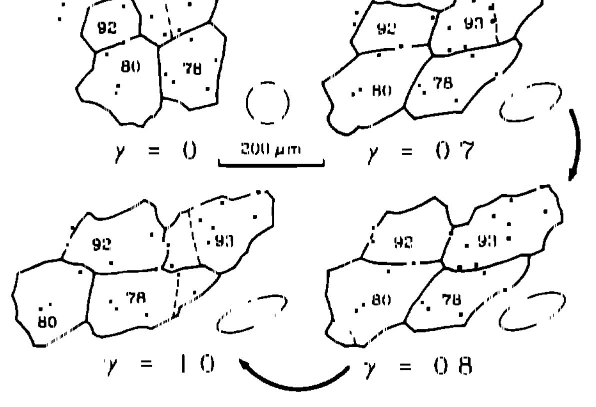

Fig 10. Foliation weakening by the migration of straight or slightly wavy grain boundaries Some of marker particles (dots) are drawn for reference. Local bulk strain ellipse is drawn in the bottom right of each stage See text for discussion

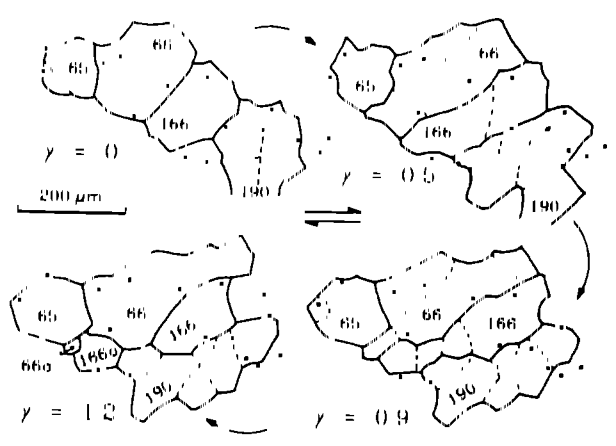

Fig 11 Foliation weakening by dissection Grain 166 is separated by growth of grains 66 and 190 Grain 66, in turn, is dissected by growth of grains 166a and 65 Dots represent marker particles The value of γ in the bottom left of each stage represents the bulk shear strain of the whole sample

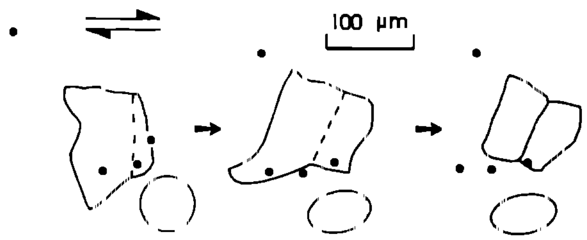

Fig 12 Foliation strengthening by the rotational recrystallization of grain 143 Ellipses indicate local bulk strains. Dashed lines represent subgrain boundaries

Acknowledgements—I thank W D Means for his invaluable advice and encouragement P D Bons helped to clarify some ambiguous points, P J Hudleston, J L Urai and M W Jessell are specially thanked for their thorough reviews and comments. The program GBO was developed jointly by me and Y. D Park This work was supported by NSF Grant EAR 8803096 to W D Means

REFERENCES

Berthé, D , Choukroune, P & Jégouzo, P 1979 Orthogneiss, mylonite and non-coaxial deformation of granites, the example of the South Armorican shear zone *J Struct. Geol* 1, 31–42

Burg, J P , Wilson, C J L & Mitchell, J C 1986 Dynamic recrystallization and fabric development during simple shear deformation of ice *J Struct Geol* 8, 857–870

Drury, M R & Urai, J L 1990 Deformation related recrystallization processes *Tectonophysics* 172, 235–253.

Hobbs, B E , Means, W D & Williams, P F 1976 *An Outline of Structural Geology* Wiley, New York.

Jessell, M W 1986 Grain boundary migration and fabric development in experimentally deformed octachloropropane *J Struct Geol* 8, 527–542

Knipe, R J & Law, R D 1987 The influence of crystallographic orientation and grain boundary migration on microstructural and textural evolution in an *S–C* mylonite *Tectonophysics* 135, 155–169

Law, R D 1986 Relationships between strain and quartz crystallographic fabrics in the Roche Maurice quartzites of Plougastel, Western Brittany *J Struct Geol* 8, 494–516

Lister, G S & Snoke, A W 1984 S–C mylonites *J. Struct Geol* 6, 617–639

Means, W D 1981 The concept of steady state foliation *Tectonophysics* 78, 179–199

Means, W D 1983 Microstructure and micromotion in recrystallization flow of octachloropropane a first look *Geol Rdsch* 72, 511–528

Means, W. D. 1989. Synkinematic microscopy of transparent polycrystals. *J. Struct. Geol.* **11**, 163–174.
Means, W. D. 1990. Review Paper—Kinematics, stress, deformation and material behavior. *J. Struct. Geol.* **12**, 953–971.
Means, W. D. & Ree, J. H. 1988. Seven types of subgrain boundaries in octachloropropane. *J. Struct. Geol.* **10**, 765–770.
Means, W. D. & Ree, J. H. 1990. Structural motion, particle motion, and migration processes in deformed materials. *Geol. Soc. Am. Abs. w. Prog.* **22**, A138.
Odling, N. E. 1984. Strain analysis and strain path modelling in the Loch Tollie gneisses, Gairloch, NW Scotland. *J. Struct. Geol.* **6**, 543–562.
Panozzo, R. 1983. Two dimensional analysis of shape fabric using projections of lines in a plane. *Tectonophysics* **95**, 279–294.
Panozzo, R. 1984. Two dimensional strain from the orientation of lines in a plane. *J. Struct. Geol.* **6**, 215–221.
Ramsay, J. G. & Graham, R. H. 1970. Strain variation in shear belts. *Can. J. Earth Sci.* **7**, 786–813.
Ramsay, J. G. & Huber, M. I. 1983. *The Techniques of Modern Structural Geology, Volume 1. Strain Analysis.* Academic Press, London.
Ree, J. H. 1988. Evolution of deformation induced grain boundary voids in octachloropropane. *Geol. Soc. Am. Abs. w. Prog.* **20**, A213.
Ree, J. H. 1990. High temperature deformation of octachloropropane: dynamic grain growth and lattice reorientation. In: *Deformation Mechanisms, Rheology and Tectonics* (edited by Knipe, R. J. & Rutter, E. H.). *Spec. Publs geol. Soc. Lond.* **54**, 363–368.
Schmid, S. M., Panozzo, R. & Bauer, S. 1987. Simple shear experiments on calcite rocks: rheology and microfabric. *J. Struct. Geol.* **9**, 747–778.
Simpson, C. & Schmid, S. M. 1983. An evaluation of the criteria to deduce the sense of movement in sheared rocks. *Bull. geol. Soc. Am.* **94**, 1281–1288.
Urai, J. L., Means, W. D. & Lister, G. S. 1986. Dynamic recrystallization of minerals. In: *Minerals and Rock Deformation: Laboratory Studies—The Paterson Volume* (edited by Heard, H. C. & Hobbs, B. E.). *Am. Geophys. Un. Geophys. Monogr.* **36**, 161–199.